nature nanotechnology

LETTERS

PUBLISHED ONLINE: 28 SEPTEMBER 2015 | DOI: 10.1038/NNANO.2015.220

A carbon nanotube optical rectenna

Asha Sharma[1,2†], Virendra Singh[1†], Thomas L. Bougher[1†] and Baratunde A. Cola[1,3*]

An optical rectenna—a device that directly converts free-propagating electromagnetic waves at optical frequencies to direct current—was first proposed over 40 years ago[1], yet this concept has not been demonstrated experimentally due to fabrication challenges at the nanoscale[2,3]. Realizing an optical rectenna requires that an antenna be coupled to a diode that operates on the order of 1 pHz (switching speed on the order of 1 fs). Diodes operating at these frequencies are feasible if their capacitance is on the order of a few attofarads[3,4], but they remain extremely difficult to fabricate and to reliably couple to a nanoscale antenna[2]. Here we demonstrate an optical rectenna by engineering metal–insulator–metal tunnel diodes, with a junction capacitance of ~2 aF, at the tip of vertically aligned multiwalled carbon nanotubes (~10 nm in diameter), which act as the antenna[5,6]. Upon irradiation with visible and infrared light, we measure a d.c. open-circuit voltage and a short-circuit current that appear to be due to a rectification process (we account for a very small but quantifiable contribution from thermal effects). In contrast to recent reports of photodetection based on hot electron decay in a plasmonic nanoscale antenna[7,8], a coherent optical antenna field appears to be rectified directly in our devices, consistent with rectenna theory[4,9,10]. Finally, power rectification is observed under simulated solar illumination, and there is no detectable change in diode performance after numerous current–voltage scans between 5 and 77 °C, indicating a potential for robust operation.

A single-frequency energy conversion efficiency greater than 90% has been demonstrated[11] for a rectenna operating at much lower frequencies in the microwave spectrum (~2 GHz). Theory suggests[9,10] that efficiencies this high could also be achieved for an optical rectenna using an ideal diode—that is, one with ultralow capacitance and resistance, and high nonlinearity and asymmetry. The cutoff frequency for a rectenna is defined[4] as $f_c = 1/(2\pi R_A C_D)$ when the diode resistance is much greater than the antenna resistance, where R_A is the antenna resistance and C_D is the capacitance of the rectenna diode. This assumption is probably appropriate for nanoscale rectenna because, although a number of efficient designs for optical antennas exist[12], contact and quantum resistances are typically large in nanoscale devices[13]. Because the diode capacitance is given by $C_D = \varepsilon_0 \varepsilon A/d$ (ref. 4), where ε_0 is the permittivity of vacuum, ε is the relative permittivity of the insulator, A is the area and d the insulator thickness, reducing the diode area is a simple approach to increase the cutoff frequency and produce an optical rectenna.

A natural approach for efficient antenna–diode coupling is to use one electrode in a metal–insulator–metal (M-I-M) diode[2,3] as the antenna. Carbon nanotubes can be used to absorb electromagnetic radiation in essentially the entire electromagnetic spectrum by both free carrier (intraband) and excitonic (interband) absorption processes[14–16], which, when combined with high carrier mobilities, makes them especially suited for broadband photonic and optoelectronic applications[17,18]. In contrast to single-walled carbon nanotubes, which can be semiconducting or metallic based on their chirality, multiwalled carbon nanotubes (MWNTs) exhibit metallic properties[19] due to the presence of at least one metallic chirality and do not typically show an excitonic photovoltaic effect[15]. The photoresponse of metallic nanotubes is usually caused by thermal effects[15]. However, the ability of metallic nanotubes to behave as antennas[5,6], coupled with their small tip area, make these materials ideal candidates for the fabrication of a combined antenna–rectifying diode (a rectenna, Fig. 1a).

Vertically aligned arrays of MWNTs were grown by chemical vapour deposition, and MWNT-I-M tunnel diodes were fabricated at the nanotube tips using atomic layer deposition (ALD) of Al_2O_3 (Fig. 1b,c) and thermal evaporation of a semi-transparent low-workfunction top metal electrode (Fig. 1b; see Methods). Our device structure (MWNT-Al_2O_3-Ca) is analogous to numerous metal whisker point contact diodes[4,20] connected in parallel, because the MWNTs are vertically aligned, physically isolated from each other by the conformal Al_2O_3 coating (Fig. 1b,c), and connected to an approximately planar top metal contact film (Fig. 1b). An insulator typically needs to be less than ~2 nm thick to allow significant electron tunnelling and rectification[21], but the intrinsic electric field (the field due to asymmetric metal workfunctions) is enhanced (Fig. 2a) at the MWNT tips in our device geometry, similar to the field enhancement that occurs in nanotube field emitters[22], which produces an estimated effective insulating barrier thickness of 1.5 nm for a deposited Al_2O_3 thickness of 8 nm (Supplementary Figs 1–4). We note that the actual atomic interfaces may be separated by a distance smaller than 8 nm due to diffusion of top metal atoms into the oxide during deposition (Supplementary Fig. 4 shows an effective insulating barrier thickness of 2.8 nm for a deposited Al_2O_3 thickness of 8 nm in a planar device with similar contrast in workfunction). The rectification asymmetry is also enhanced (Supplementary Fig. 5) and the turn-on voltage decreased (Fig. 2b and Supplementary Fig. 1) by the large difference in workfunction between the MWNTs (Supplementary Fig. 6) and Ca. The MWNT-Al_2O_3-Ca diode has a workfunction difference of 2.1 eV, whereas the diode with an Al top metal has a workfunction difference of only 0.7 eV. Note that devices with the Al top metal contact did not produce a detectable photoresponse in our testing due to their high turn-on voltages.

Given that electron transport is most efficient in the axial direction of MWNTs[19,23], the diode area where electron tunnelling occurs is probably defined by the outer MWNT tip diameter of 8–10 nm, as illustrated in Fig. 1a. Thus, the diode capacitance is inherently on the order of a few attofarads in our design, which enables operation at petahertz frequencies. To confirm this, specific capacitances on the order of $3 \pm 0.6\ \mu F\ cm^{-2}$ for entire devices, or ~2 aF per MWNT junction, are extracted from capacitance measurements in a standard low-frequency range (Fig. 2c) by using the number density of MWNTs ($\sim 10^{10}\ cm^{-2}$) to determine the real or active

[1]George W. Woodruff School of Mechanical Engineering, Georgia Institute of Technology, Atlanta, Georgia 30332, USA. [2]Center for Organic Photonics and Electronics, School of Electrical & Computer Engineering, Georgia Institute of Technology, Atlanta, Georgia 30332, USA. [3]School of Materials Science and Engineering, Georgia Institute of Technology, Atlanta, Georgia 30332, USA. †These authors contributed equally to this work. *e-mail: cola@gatech.edu

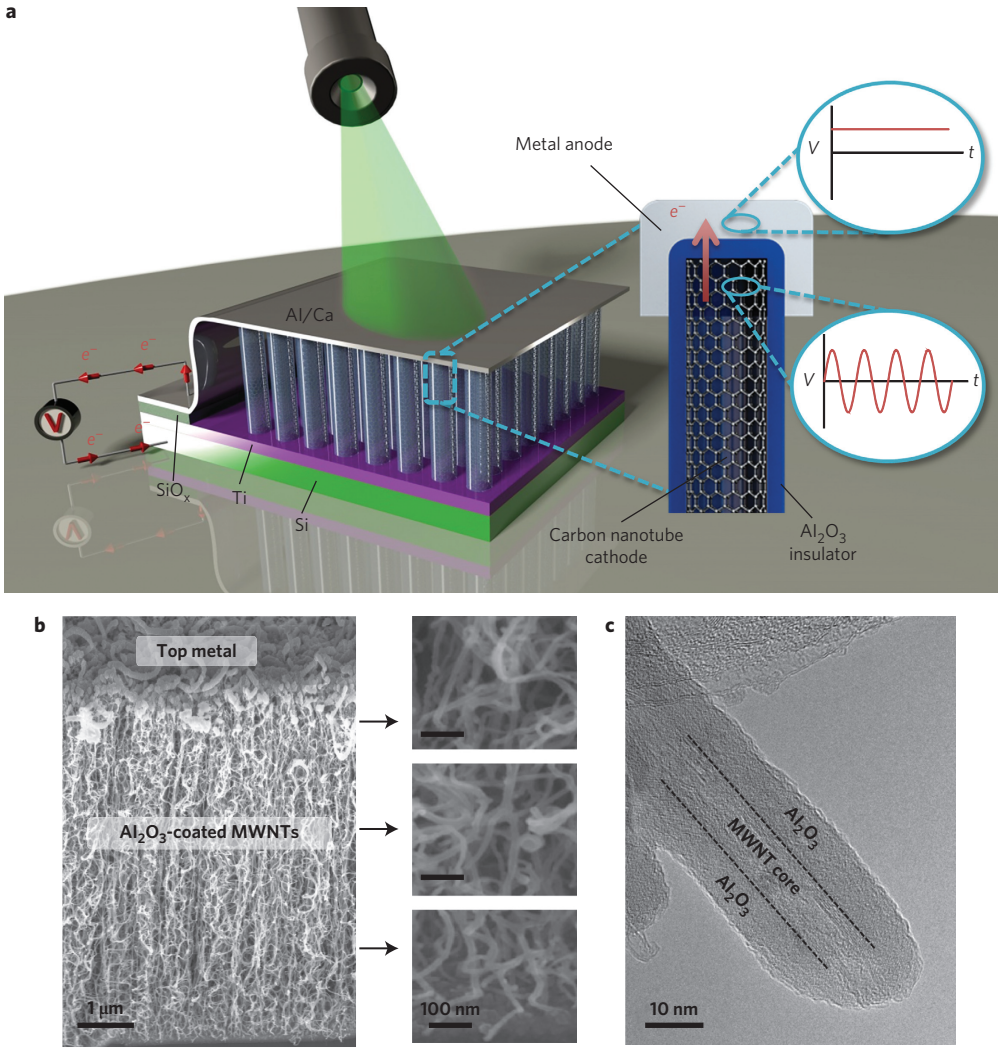

Figure 1 | Carbon nanotube optical rectenna. a, Schematic of the vertically aligned MWNT-I-M optical rectenna. MWNTs are supported on a low-resistivity Si substrate with a back metal (Ti) contact, coated with an insulator (Al_2O_3) from roots to tips and topped with a 40 nm Ca/20 nm Al semi-transparent electrode. An insulating SiO_x layer is deposited between the Ti and top electrode for current and voltage measurements on the area to the left of the MWNTs. The device is illuminated from the top with laser or solar light. The effective diode structure at the tip of a single MWNT is shown to the right of the device. The red arrow indicates the direction of electron (e^-) emission from the MWNT cathode into the top metal anode. Right: a.c. input voltage signal in the MWNT antenna and d.c. voltage output signal in the top metal anode after rectification in the diode. **b**, Scanning electron micrograph (SEM) of a representative MWNT-I-M device. The MWNT array density is ~10^{10} cm^{-2}. Right: zoomed-in images of the bottom, middle and top regions of the oxide-coated MWNTs. **c**, Transmission electron micrograph (TEM) of a representative oxide-coated MWNT. The oxide coating is 8 nm thick. Dotted black lines show the interface of the MWNT and oxide coating.

device area, which is about 200 times smaller than the apparent device area. From the capacitance measurements we estimate a relative permittivity of 3.8 for the Al_2O_3 layer, which agrees with reports for Al_2O_3 (deposited by ALD) in this thickness range[24] (Supplementary Section 3 and Supplementary Fig. 7). The inset in Fig. 2c shows that the capacitance of the MWNT-I-M diodes is stable from at least −2 to 2 V, which is important for robust device operation. Although thicker oxide produces lower capacitance (Fig. 2c), this is not a viable approach to increase the device cutoff frequency because of the associated increase in resistance, which diminishes the current and nonlinearity in the diode (Fig. 2d and Supplementary Fig. 8). The current–voltage characteristics, $I(V_{dc})$, of our MWNT-I-M diodes show rectified currents up to 2 A cm^{-2} at less than 1 V applied bias (Fig. 2b) and are consistent over numerous scans on the same device and for several different devices created from similar MWNT arrays (Fig. 2b and Supplementary Fig. 9). In addition, the current–voltage characteristics show little temperature dependence from 5 to 77 °C (Fig. 2e), indicating that there are no detectable effects from thermal expansion in our devices, and that our devices do not behave as semiconductor-based diodes or semiconducting nanotube Schottky junctions, which are known to have strong temperature dependence[25].

Our MWNT rectenna devices show increased nonlinearity and reduced zero-bias differential resistance when illuminated (Fig. 3, Supplementary Fig. 10 and Supplementary Table 1), in agreement with expectations based on photon-assisted tunnelling (Supplementary equations (9) and (10)). The photoresponse (photocurrent divided by the illumination power) of our devices (Fig. 3a) to 532 nm light is higher than the response to 1,064 nm light (5 A W^{-1} for 532 nm and 1.4 A W^{-1} for 1,064 nm, at 1.25 V), which also agrees with expectations based on photon-assisted tunnelling. The photoresponse of our devices is at least six orders of magnitude higher than in previous optical rectification studies

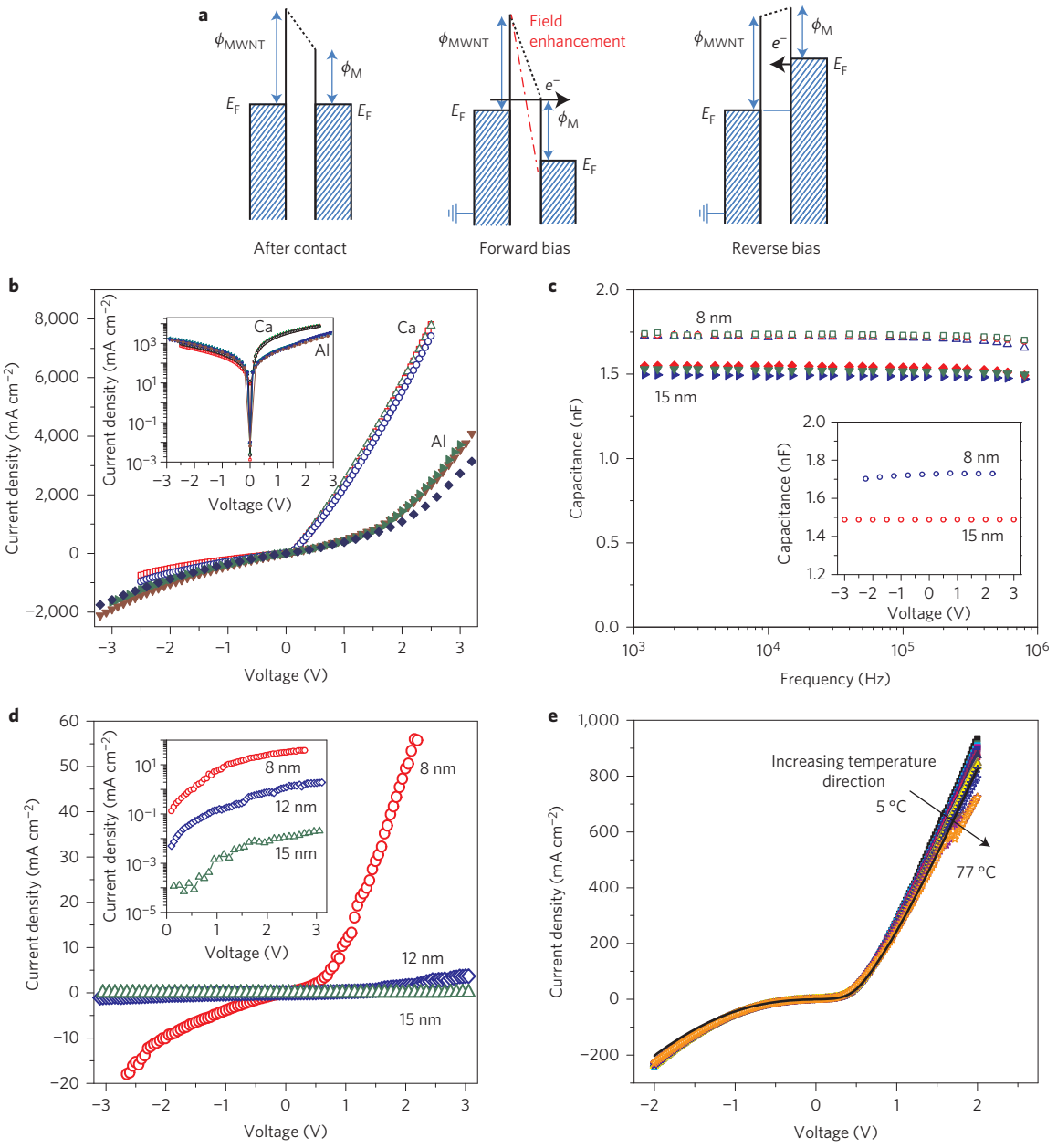

Figure 2 | MWNT-I-M tunnel diode characteristics. a, An approximate potential energy level diagram for an asymmetric tunnel diode with MWNT-I-M structure. The dash-dotted red line shows the reduced effective barrier thickness due to geometric field enhancement in the diode at the MWNT tips. The Fermi level is denoted E_F and ϕ is the workfunction (subscripts 'MWNT' and 'M' indicate MWNT and metal, respectively). The flow of electrons near the Fermi level is denoted by the direction of the black arrow and e^-. **b**, Comparison of current–voltage characteristics of MWNT-I-M vertical diode array devices using lower-workfunction metal (Ca, workfunction of 2.9 eV) and higher-workfunction metal (Al, workfunction of 4.3 eV). Inset: semi-logarithmic plots of the data. The multiple traces for the Ca and Al devices are multiple scans on the same device. **c**, Capacitance C (device area = 0.1 cm^2) of MWNT-I-M (MWNT-Al_2O_3-Ca) structures with 8 nm and 15 nm Al_2O_3 as a function of frequency at 20 mV_{rms}. The multiple traces are multiple scans on the same device. Inset: Voltage stability of the devices. **d**, Current–voltage characteristics of tunnel diodes using 8, 12 and 15 nm Al_2O_3. Inset: semi-logarithmic plots of the data. **e**, Temperature-dependent current–voltage characteristics of MWNT-I-M devices between 5 and 77 °C with increments of ~5 °C. The devices were tested again at room temperature the next day, and the corresponding curves are plotted in the same graph, showing no appreciable difference. The devices in **b**, **d** and **e** are from different MWNT batches with variations in resistances and current densities.

(Supplementary Table 2). We note that, in contrast to the photocurrent response, the open-circuit photovoltage response to 532 nm light is lower than the response to 1,064 nm light (Fig. 3b,c), which we discuss further below as evidence for rectenna operation. Our devices generate power in the second quadrant of the $I(V_{dc})$ curve, as expected[9,26] in an optical rectenna photoresponse. This highlights the different physics in our devices compared with the photovoltaic effect induced by the bandgap in semiconductors, which is known to generate power in the fourth quadrant of the device $I(V_{dc})$ curve. The measured open-circuit voltage (V_{oc}) and short-circuit current (I_{sc}) (Supplementary Table 1) agree reasonably well with the values extracted from the $I(V_{dc})$ curves in Fig. 3. The I_{sc} of our MWNT rectenna devices (Supplementary Table 1) is about 10 times smaller for broadband solar illumination than for monochromatic illumination, which is probably due to frequency mixing losses under broadband illumination[10]. This is consistent

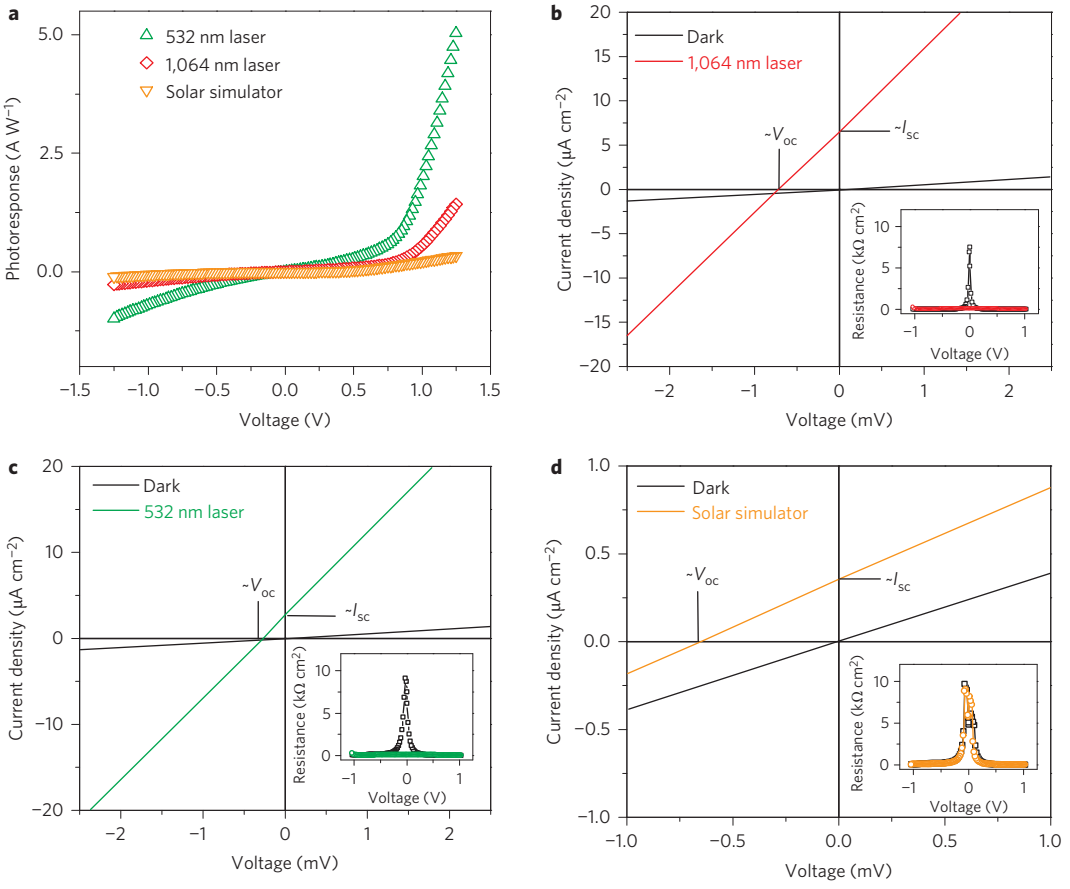

Figure 3 | Optical rectification of infrared, visible and simulated solar light. a, Photoresponse (photocurrent divided by illumination power) versus voltage of a device responding to 1.5 AM solar (100 mW cm^{-2}), 1,064 nm (92 mW cm^{-2}) and 532 nm (26 mW cm^{-2}) illumination with 10% transmission through the top metal contact. **b**–**d**, High-resolution views of the illuminated current–voltage response to 1,064 nm laser (**b**), 532 nm laser (**c**) and 1.5 AM solar illumination (**d**). The V_{oc} and I_{sc} noted in the high-resolution views of the current–voltage responses are the measured open-circuit voltage and short-circuit current for each illumination case. Insets in **b**–**d**: differential resistances.

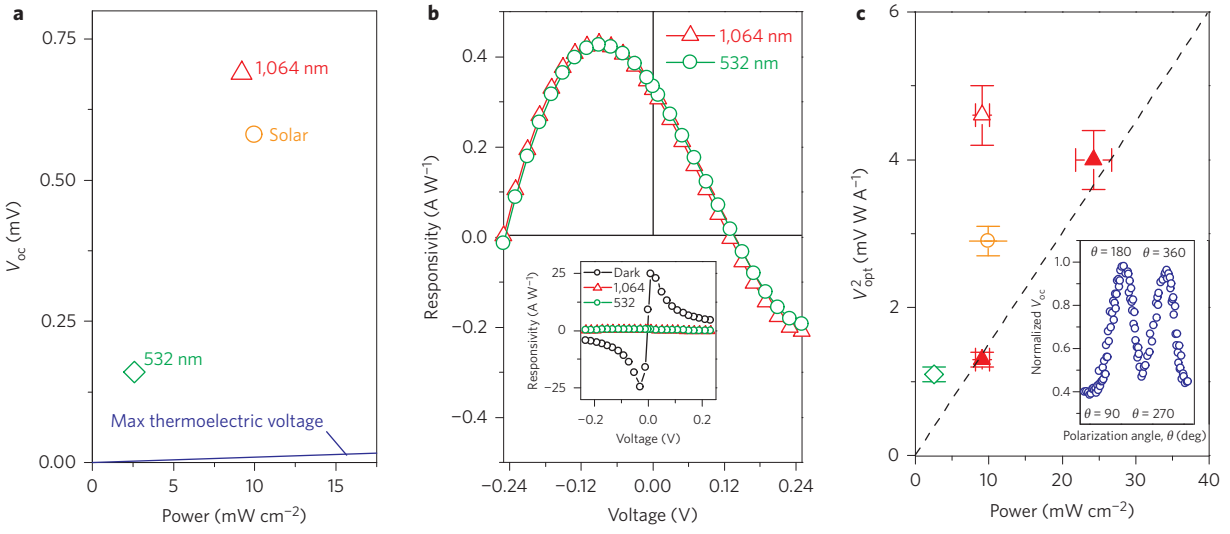

Figure 4 | Optical rectification voltage and device responsivity. a, Measured open-circuit voltage from 1.5 AM solar, 1,064 nm and 532 nm illumination versus illumination power absorbed in the MWNT rectenna device, which is 10% of the incident power based on the measured transmissivity of the semi-transparent top metal contact. Blue line: maximum possible thermoelectric voltage for the same device structures under at least 112 times higher illumination intensity. **b**, Diode responsivity under 1,064 nm and 532 nm illumination. Inset: comparison of illuminated and dark responsivity. **c**, Square of the a.c. optical antenna voltage versus illumination power absorbed in the MWNT rectenna device. V^2_{opt} is equal to two times V_{oc} times the inverse of diode responsivity at zero bias (Supplementary Section 5). Open symbols are from the devices in Fig. 3 and filled symbols are for a device from a different batch of MWNTs with higher diode resistances. The vertical error bars are the measured range of variation in illumination power and the horizontal error bars represent three to five measurements on the same device. Inset: polarization dependence of the rectified voltage.

with the higher zero-bias resistance under solar illumination (Fig. 3d, inset) compared with laser illumination (Fig. 3b,c, insets).

Thermal effects can hamper clear identification of a rectification photoresponse[27]. The asymmetry in our MWNT-Al_2O_3-Ca tunnel junctions could produce significant thermal voltages[27], but we do not expect this in our testing, where illumination is diffused over centimetre-sized areas and is about 10,000 times less intense than intensities used in a previous optical rectification study[26]. The maximum photon energy in our tests is below the energy required to sustain excited electrons in the conduction band of amorphous AlO_x[28], which is required to produce significant photocurrent based on hot-electron transport in M-I-M diodes[29,30]. To isolate possible thermoelectric effects in carbon nanotubes[17,18] on the measured photoresponse of our devices, we modified our devices with an opaque Al capping layer (150 nm thick) to prevent an optical rectification response, and heated them with a 532 nm laser with an intensity of 11.2 W cm^{-2}, about 112 times more intense than the maximum intensity in our rectenna response tests. The magnitude and sign of the measured voltage changes with the position of the heating spot with respect to the contacts (Supplementary Fig. 12), which is consistent with a thermoelectric effect[17,18]. The maximum thermoelectric response based on 112 times higher illumination intensity is less than 1% of the measured optical rectification V_{oc} for 1,064 nm, 532 nm and solar illumination (Fig. 4a). The distance between contacts in our vertical device architecture (~10 μm) is much smaller than those used in horizontally aligned carbon nanotube photodetectors based on the thermoelectric effect (~1 mm)[18], which makes it difficult to support a significant temperature gradient at illumination intensities of ~100 mW cm^{-2}. Additionally, the change in nonlinearity in the $I(V_{dc})$ curves for our devices (Fig. 3) is not observed in a thermoelectric response[17,18], where the $I(V_{dc})$ curve remains linear under illumination.

Using diode characteristics extracted from the illuminated $I(V_{dc})$ curves as discussed above, the change in diode responsivity with voltage is shown in Fig. 4b for the same device under 1,064 nm and 532 nm laser illumination. The decrease in responsivity with monochromatic illumination compared to the dark diode characteristics could be the result of photo-excited electrons tunnelling with higher probability under reverse bias (Fig. 2a), due to the much higher carrier concentration in metals than in MWNTs. There is a minor change in the responsivity under solar illumination when compared with dark conditions, except near the zero-bias condition where there is a significant decrease (Supplementary Table 1). Using the zero-bias responsivity under illumination to normalize V_{oc}, the voltage response to 1,064 nm illumination on the same device appears to scale linearly with illumination power and intercepts the origin (Fig. 4c) as expected. This normalization is equivalent to the square of the a.c. optical voltage (V_{opt}^2) (Supplementary Section 5), which is proportional to the power received by the MWNT antenna[4]. Additionally, the measured V_{oc} is polarization-dependent (Fig. 4c, inset), which is consistent with the MWNTs behaving as classical antennas[5,6]. The results in Fig. 4 indicate that, despite the slightly higher illumination power, the optical voltage under solar illumination is significantly less than the optical voltage under 1,064 nm laser illumination, and a larger photon energy does not necessarily produce a larger optical voltage without consideration of the illumination power, and probably the degree of illumination coherence. These findings appear to agree qualitatively with the rectenna V_{oc} predicted by a recent thermodynamic analysis[31]. Additionally, the $\partial^2 I/\partial V^2$ computed from the illuminated $I(V_{dc})$ curve to approximate the required quantum correction is directly proportional to photocurrent in our devices (Supplementary Fig. 13), which is additional evidence for the optical rectification mechanism[26].

The inferred V_{opt} values for solar, 1,064 nm and 532 nm illumination are 52, 68 and 33 mV, respectively (Fig. 3 devices). These optical voltages are of the same order as the optical voltages drawn from rectification in a symmetric gold vacuum tunnel junction under 10,000 times greater illumination intensity[26], which suggests that the optical coupling to our MWNT antenna could be more efficient due to collective antenna coupling in the arrays[5,6]. However, further experimental and theoretical work is required to fully understand the generation and rectification of optical voltage in MWNT arrays and to characterize the effective antenna resistance. These studies are required to estimate an efficiency limit (based on Supplementary equation (11)) and a precise cutoff frequency for our rectenna devices. Our results, however, demonstrate operation at 564 THz, which is supported by the extremely low capacitance of our diodes (~2 aF, which using a conservative antenna resistance estimate of 100 Ω, the range of values for a single metal whisker antenna[4] with no enhancement from collective effects as in our devices, gives a cutoff frequency of ~800 THz). Considering the number density of MWNTs in the arrays (~10^{10} cm^{-2}), the resistance of a single MWNT-I-M junction is on the order of 1 TΩ, which is several orders of magnitude higher than the resistance of typical MWNT interconnects[13]. Our device junction resistances are higher because they include the intrinsic resistance of the oxide-coated MWNT and contact resistances, and the resistance of the oxide barrier, which increases exponentially with the oxide thickness in a tunnel diode[21]. The high electrical resistance of a single MWNT-I-M junction probably creates poor impedance matching with the MWNT antenna, which limits the rectified power in a single junction[3] and is a major issue to focus on for future improvements. The large number density of MWNT-I-M diodes connected in parallel, however, substantially increases current and power production at the device level. The measured power conversion efficiency of our MWNT array rectenna device is ~10^{-5}% under 1,064 nm laser illumination (Supplementary Table 1), which is the highest efficiency measured in our present devices. However, this conversion efficiency appears to be limited by the quality and geometry of our carbon nanotubes and other fabrication challenges rather than predicted fundamental limits[9,10], and could be increased dramatically with more efficient optical voltage coupling, thinner insulator barriers and low-resistance electrical contacts to the MWNTs. Improving our device in these ways could provide definitive evidence of the optical rectenna mechanism as well as practical applications.

Methods

Methods and any associated references are available in the online version of the paper.

Received 26 May 2015; accepted 24 August 2015;
published online 28 September 2015

References

1. Bailey, R. L. A proposed new concept for a solar-energy converter. *J. Eng. Power* **94,** 73–77 (1972).
2. Donchev, E. *et al.* The rectenna device: from theory to practice (a review). *MRS Energy Sustain.* **1,** 1–34 (2014).
3. Moddel, G. & Grover, S. *Rectenna Solar Cells* (Springer, 2013).
4. Sanchez, A., Davis, J. C. F., Liu, K. C. & Javan, A. The MOM tunneling diode: theoretical estimate of its performance at microwave and infrared frequencies. *J. Appl. Phys.* **49,** 5270–5277 (1978).
5. Wang, Y. *et al.* Receiving and transmitting light-like radio waves: antenna effect in arrays of aligned carbon nanotubes. *Appl. Phys. Lett.* **85,** 2607–2609 (2004).
6. Kempa, K. *et al.* Carbon nanotubes as optical antennae. *Adv. Mater.* **19,** 421–426 (2007).
7. Knight, M. W., Sobhani, H., Nordlander, P. & Halas, N. J. Photodetection with active optical antennas. *Science* **332,** 702–704 (2011).
8. Giugni, A. *et al.* Hot-electron nanoscopy using adiabatic compression of surface plasmons. *Nature Nanotech.* **8,** 845–852 (2013).
9. Sachit, G., Saumil, J. & Garret, M. Quantum theory of operation for rectenna solar cells. *J. Phys. D* **46,** 135106 (2013).

10. Joshi, S. & Moddel, G. Efficiency limits of rectenna solar cells: theory of broadband photon-assisted tunneling. *Appl. Phys. Lett.* **102,** 083901 (2013).
11. Brown, W. C. Optimization of the efficiency and other properties of the rectenna element. In *Proc. Microwave Symposium, 1976 IEEE-MTT-S International* 142–144 (1976).
12. Novotny, L. & van Hulst, N. Antennas for light. *Nature Photon.* **5,** 83–90 (2011).
13. Songkil, K. *et al.* Fabrication of an ultralow-resistance ohmic contact to MWCNT–metal interconnect using graphitic carbon by electron beam-induced deposition (EBID). *IEEE Trans. Nanotechnol.* **11,** 1223–1230 (2012).
14. Avouris, P., Freitag, M. & Perebeinos, V. Carbon-nanotube photonics and optoelectronics. *Nature Photon.* **2,** 341–350 (2008).
15. Barkelid, M. & Zwiller, V. Photocurrent generation in semiconducting and metallic carbon nanotubes. *Nature Photon.* **8,** 47–51 (2014).
16. Nanot, S., Hároz, E. H., Kim, J.-H., Hauge, R. H. & Kono, J. Optoelectronic properties of single-wall carbon nanotubes. *Adv. Mater.* **24,** 4977–4994 (2012).
17. Nanot, S. *et al.* Broadband, polarization-sensitive photodetector based on optically thick films of macroscopically long, dense, and aligned carbon nanotubes. *Sci. Rep.* **3,** 1335 (2013).
18. He, X. *et al.* Carbon nanotube terahertz detector. *Nano Lett.* **14,** 3953–3958 (2014).
19. Frank, S., Poncharal, P., Wang, Z. L. & de Heer, W. A. Carbon nanotube quantum resistors. *Science* **280,** 1744–1746 (1998).
20. Daneu, V., Sokoloff, D., Sanchez, A. & Javan, A. Extension of laser harmonic-frequency mixing techniques into the 9 μ region with an infrared metal–metal point-contact diode. *Appl. Phys. Lett.* **15,** 398–401 (1969).
21. Simmons, J. G. Electric tunnel effect between dissimilar electrodes separated by a thin insulating film. *J. Appl. Phys.* **34,** 2581–2590 (1963).
22. Xu, X. & Brandes, G. A method for fabricating large-area, patterned, carbon nanotube field emitters. *Appl. Phys. Lett.* **74,** 2549–2551 (1999).
23. Ebbesen, T. W. *et al.* Electrical conductivity of individual carbon nanotubes. *Nature* **382,** 54–56 (1996).
24. De Heer, W. A., Châtelain, A. & Ugarte, D. A carbon nanotube field-emission electron source. *Science* **270,** 1179–1180 (1995).
25. Appenzeller, J., Radosavljević, M., Knoch, J. & Avouris, P. Tunneling versus thermionic emission in one-dimensional semiconductors. *Phys. Rev. Lett.* **92,** 048301 (2004).
26. Ward, D. R., Huser, F., Pauly, F., Cuevas, J. C. & Natelson, D. Optical rectification and field enhancement in a plasmonic nanogap. *Nature Nanotech.* **5,** 732–736 (2010).
27. Tu, X. W., Lee, J. H. & Ho, W. Atomic-scale rectification at microwave frequency. *J. Chem. Phys.* **124,** 021105 (2006).
28. Kovacs, D. A., Winter, J., Meyer, S., Wucher, A. & Diesing, D. Photo and particle induced transport of excited carriers in thin film tunnel junctions. *Phys. Rev. B* **76,** 235408 (2007).
29. Chalabi, H., Schoen, D. & Brongersma, M. L. Hot-electron photodetection with a plasmonic nanostripe antenna. *Nano Lett.* **14,** 1374–1380 (2014).
30. Wang, F. & Melosh, N. A. Plasmonic energy collection through hot carrier extraction. *Nano Lett.* **11,** 5426–5430 (2011).
31. Lerner, P. B., Miskovsky, N. M., Cutler, P. H., Mayer, A. & Chung, M. S. Thermodynamic analysis of high frequency rectifying devices: determination of the efficiency and other performance parameters. *Nano Energy* **2,** 368–376 (2013).

Acknowledgements

This work was supported by the Defense Advanced Research Projects Agency under Young Faculty Award grant no. N66001-09-1-2091 (Program manager: Nibir Dhar) and by the Army Research Office under Young Investigator Program agreement no. W911NF-13-1-0491 (Program manager: William W. Clark). The authors thank S. Singh for help with metal deposition, B. Kippelen for providing access to testing facilities and several colleagues for helpful discussions.

Author contributions

B.A.C. conceived the rectenna device and wrote the manuscript with comments and edits from all authors. A.S. and V.S. fabricated the devices and characterized materials. A.S. measured the rectenna response on all devices. T.L.B. performed device modelling and thermoelectric response experiments. All authors contributed to data analysis and interpretation.

Additional information

Supplementary information is available in the online version of the paper. Reprints and permissions information is available online at www.nature.com/reprints. Correspondence and requests for materials should be addressed to B.A.C.

Competing financial interests

Georgia Tech has applied for a patent, application no. PCT/US2013/065918, related to the design methods and materials produced in this work.

Methods

Device fabrication. Vertically aligned arrays (density ~10^{10} cm^{-2}) of MWNTs were grown on Si substrates using a low-pressure chemical vapour deposition (LPCVD) process at 850 °C and 1 kPa in an Aixtron Black Magic reactor with C_2H_2 as the carbon source gas. Ti, Al and Fe films with thicknesses of 100, 10 and 3 nm were evaporated onto the Si as support and catalyst layers for MWNT growth. To allow probing away from the active area of the devices, a SiO_x barrier layer (250 nm) was deposited on half of the Si substrate (Fig. 1a). A growth time of between 1 and 3 min produced MWNTs with average heights of ~10 μm. Scanning and transmission electron microscopy were used to characterize the structure of the MWNTs and their coatings. The average diameters of the MWNTs were ~8–10 nm, and the average number of walls is six (Fig. 1c). Al_2O_3 dielectric layers of 8, 12 or 15 nm were deposited on the MWNTs by ALD at 250 °C using trimethylaluminium (TMA) and water (H_2O) vapours. These thicknesses are based on optimized ALD cycles (100 cycles = 10 nm), which were calibrated on planar Si substrates. Purge times of 30 s were used in each ALD cycle for both TMA and H_2O to enable the TMA and H_2O vapour to diffuse completely from the MWNT tips to the substrate base. Between two sets of ALD, oxygen plasma was used to oxidize the surface of the MWNTs and introduce hydrophilic moieties[16,17] (–OH and –COOH), which promote uniform nucleation (Fig. 1b,c) and conformal deposition of Al_2O_3 on the MWNTs. A semitransparent metal top contact of Ca (40 nm)/Al (20 nm) or opaque 100 nm Al for the device in Fig. 2b,e was then vacuum (base pressure less than 10^{-7} torr) deposited on the arrays using a shadow mask to form the MWNT rectenna devices. The source metals were from Lesker and had a purity of 99% or greater. The Al layer was required to prevent or minimize oxidation of Ca in air.

Electrical measurements. The current–voltage $I(V_{dc})$ characteristics of the MWNT-I-M rectenna were measured using an Agilent E5272A source monitor unit connected to a d.c. electrical probing station with a temperature-controlled stage. The resistance of the probe and lead wires was on the order of 1 Ω. Capacitance–frequency characteristics were measured using an HP 4284 capacitance meter at room temperature. The capacitance and the operating electric field strength limits in the MWNT-I-M devices were established by measuring the specific capacitances as a function of d.c. bias for oxide thicknesses of 8 and 15 nm at a frequency of 10^5 Hz and 20 mV_{rms}. The workfunctions of the MWNTs were measured in air using a Kelvin probe (Besocke Delta Phi) with reference to a highly ordered pyrolytic graphite crystal sample. Electrical and optical tests were performed in a glove box under a nitrogen environment and at near atmospheric pressure and temperature, except for the temperature-dependent current–voltage scans.

Optical measurements. An infrared continuous waveform laser with a wavelength of 1,064 nm (282 THz) at intensities of 92 mW cm^{-2} and 243 mW cm^{-2}, a green continuous waveform laser with a wavelength of 532 nm (564 THz) at an intensity of 26 mW cm^{-2}, and an AM 1.5 solar simulation source with an intensity of 100 mW cm^{-2} were used to test the rectenna response. Our MWNT arrays were ~10 μm in height, which is much longer than the wavelengths of illumination, so they respond as antenna in the resistive limit[4] rather than being resonant at the test frequencies. The angle of illumination was aligned to the surface normal, except in measurements as a function of polarization, as discussed in the following. The estimated transmissivity of the top metal contact (40 nm Ca/20 nm Al) for the tested wavelengths was 10% based on measurements with the same contact film composition on a transparent substrate. The polarization of the infrared laser (the output is linearly polarized) was controlled using a half waveplate and a linear polarizer. The open-circuit voltage response as a function of polarization was measured by rotating the polarization angle of the laser beam with respect to the MWNT antenna alignment and aligning the illumination at 45° from the surface normal. All measurements were performed at room temperature.